Capture into resonance and phase-space dynamics in an optical centrifuge

Tsafrir Armon and Lazar Friedland*
Racah Institute of Physics, Hebrew University of Jerusalem, Jerusalem 91904, Israel
(Received 8 February 2016; published 7 April 2016)

The process of capture of a molecular ensemble into rotational resonance in the optical centrifuge is investigated. The adiabaticity and phase-space incompressibility are used to find the resonant capture probability in terms of two dimensionless parameters $P_{1,2}$ characterizing the driving strength and the nonlinearity, and related to three characteristic time scales in the problem. The analysis is based on the transformation to action-angle variables and the single resonance approximation, yielding reduction of the three-dimensional rotation problem to one degree of freedom. The analytic results for capture probability are in good agreement with simulations. The existing experiments satisfy the validity conditions of the theory.

DOI: 10.1103/PhysRevA.93.043406

I. INTRODUCTION

The field of optical control and manipulation of molecular rotation has seen major advances over the years, and today various techniques allow one to control the rotation alignment [1,2], orientation [3,4], and directionality [5–7] of molecular ensembles. One of the most innovative tools in this field is the *optical centrifuge* (OC), originally proposed and implemented by Corkum and collaborators [8,9], who introduced the possibility of controlled excitation of the molecular rotational degree of freedom by chirped laser pulses. The controlled nature of this process is twofold: the molecules reach very high rotational states (*super-rotors*), but they also remain closely centered around a specific target energy or frequency. The controlled rotation could be used to selectively dissociate molecules [9] or a specific molecular bond [10] and has been shown to change molecular characteristics, such as the molecule's stability against collisions [11] and its scattering from surfaces [12]. Furthermore, a gas of super-rotors may exhibit new optical properties [13] and formation of vortices [14].

Over the last few years, several state-of-the-art experiments have been performed [15–17] utilizing different molecules and exploring the dynamics during and after the OC laser pulse, including the excitation process [16], the gyroscopic stage in which the molecules remain oriented [18], and the equilibration and thermalization that follows the pulse and produces an audible sound wave [19]. However, while the experimental setups improved considerably, the process of capture of molecules into the chirped resonant rotation is still poorly understood. This process was only studied numerically [20] or under the constraint that the molecules rotate in a plane perpendicular to the laser propagation axis [8,21,22]. The former assumption makes it impossible to study the response of a randomly oriented molecular ensemble to the OC pulse. As a result, the efficiency of the OC, i.e., the fraction of molecules captured by the chirped laser drive, was not analyzed sufficiently.

In this work, we show that under the rigid-rotor approximation the OC is an example within a broad family of driven nonlinear systems exhibiting a sustained phase locking or *autoresonance* (AR) with a chirped drive. This phenomenon has been observed and studied in many applications, including atomic systems [23,24], plasmas [25,26], fluids [27], and semiconductor quantum wells [28]. By using methods in the theory of AR and analyzing the associated phase-space dynamics we calculate the efficiency of the OC process. The quantum counterpart of the AR is the quantum energy ladder climbing [29–31], but we show that the classical AR analysis is relevant to many current experimental setups.

The scope of the paper is as follows. In Sec. II, we discuss the driven-chirped molecular rotation in three dimensions, transform to action-angle variables, and use the single resonance approximation to reduce the problem to one degree of freedom. Section III focuses on calculating the efficiency of the resonant capture process in the system via analyzing its dynamics in a continuous phase space instead of a single-particle approach. In Sec. IV, we compare the theory with numerical simulations and discuss the validity of our approximations and the applicability to current experimental setups. Our conclusions are summarized in Sec. V.

II. THE MODEL

A. Parametrization

The fundamental idea of the OC is that an anisotropic molecule will "chase" a rotating linearly polarized wave (and, thus, be rotationally excited), whose polarization rotation accelerates over time. In practice, such a driving wave is created by combining two counter-rotating and antichirped circularly polarized laser beams [8]. For a wave propagating along the Z axis, with polarization angle $\phi_d(t)$ in the XY plane, after averaging over the optical frequency of the laser beams, the interaction potential energy of a molecule in spherical coordinates is given by $U = -\varepsilon \sin^2\theta \cos^2(\varphi - \phi_d)$ [8], where $\varepsilon = (\alpha_\parallel - \alpha_\perp)E_0^2/4$, $\alpha_\parallel$,$\alpha_\perp$ are the polarizability components of the molecule, and E_0 is the electric field amplitude of the combined beam. For simplicity, we use a *linearly chirped* driving frequency $\omega_d = d\phi_d/dt = \beta t/2$, where $\beta > 0$ is the chirp rate, but any sufficiently slow chirp will lead to similar results. The initial rotation frequency is set by taking an appropriate initial time.

Our driven system can be characterized by three different time scales, i.e., the drive sweeping time $t_s = 1/\sqrt{\beta}$, the

*lazar@mail.huji.ac.il

characteristic thermal rotation time $t_{\rm th} = 1/\omega_{\rm th} = \sqrt{I/k_B T}$, and the driving time scale $t_d = L_{\rm th}/\varepsilon = \sqrt{I k_B T}/\varepsilon$, where T is the temperature, I is the molecule's moment of inertia, and $L_{\rm th} = I\omega_{\rm th}$ is the characteristic thermal angular momentum. These three time scales define two dimensionless parameters:

$$P_1 = \frac{t_s}{t_d} = \frac{\varepsilon}{\sqrt{I k_B T \beta}}, \tag{1}$$

which measures the drive's strength, and

$$P_2 = \frac{t_s}{t_{\rm th}} = \sqrt{\frac{k_B T}{I\beta}}, \tag{2}$$

characterizing the nonlinearity of the problem. These parameters enter naturally in the dimensionless Hamiltonian of our driven system in spherical coordinates,

$$H = \frac{P_2}{2}\left(p_\theta^2 + \frac{p_\varphi^2}{\sin^2\theta}\right) - P_1 \sin^2\theta \cos^2(\varphi - \phi_d), \tag{3}$$

where we normalize the canonical momenta and later the total angular momentum L with respect to $L_{\rm th}$ and use the dimensionless time $\tau = \sqrt{\beta}t$. The evolution equations based on this Hamiltonian comprised one of the two sets used for Monte Carlo simulations in this work. Figure 1 shows the distributions (histograms) of the normalized angular momenta at the end of the chirped OC drive after starting from an initially thermal molecular ensemble. The resonant normalized angular momentum in the OC equals the instantaneous driving frequency normalized with respect to $\omega_{\rm th}$ (see below). The initial and final normalized driving frequencies in Fig. 1 were 1 and 8, respectively, and we used parameters $P_2 = 2.51$ and $P_1 = 0.63$ [Fig. 1(a)], 2.51 [Fig. 1(b)], and 39.8 [Fig. 1(c)]. When parameter P_1 is increased (for constant P_2 this corresponds to increasing the laser intensity), more molecules experience significant acceleration. Nevertheless, if one seeks

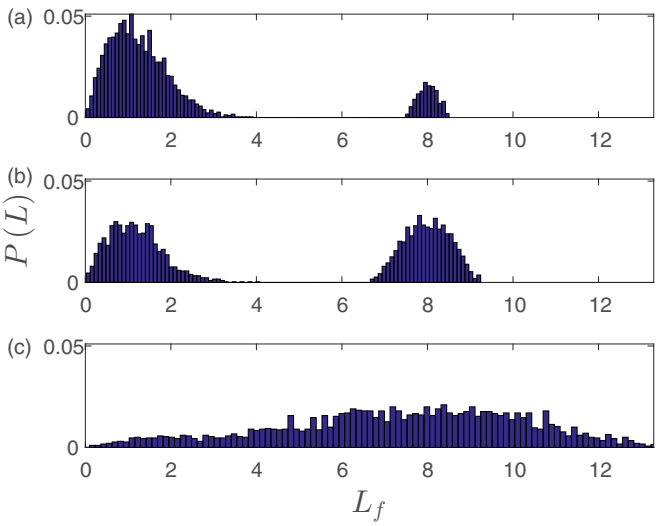

FIG. 1. Monte Carlo simulation of the distribution of angular momenta L_f for an initially thermal ensemble (3000 molecules) after the OC pulse with initial and final normalized driving frequencies $\omega_0 = 1$ and $\omega_f = 8$. The parameters are $P_2 = 2.51$ and (a) $P_1 = 0.63$, (b) $P_1 = 2.51$, and (c) $P_1 = 39.8$.

a narrow distribution around a specific target frequency, the acceleration in Figs. 1(b) and 1(c) does not provide the desired level of control, showing a broad distribution around the target. In contrast, Fig. 1(a) is a representative example for the degree of control and accuracy one can achieve with the OC, provided the parameters are chosen appropriately. In this work we calculate the excitation efficiency and the width of the final distribution of the angular momentum in the $P_{1,2}$ parameter space.

B. Transformation to action-angle variables and single-resonance approximation

Like many other physical systems, it is convenient to transform our driven problem to the action-angle variables of the unperturbed problem since the latter is integrable. This canonical transformation $\theta,\varphi,p_\theta,p_\varphi \to \Theta_L,\Theta_{L_z},L,L_z$ (see Appendix for details) leads to nontrivial angle variables (related to Euler angles), while the actions L and L_z are the normalized total angular momentum and its projection on the Z axis. The transformed Hamiltonian assumes the form

$$H(\Theta_L,\Theta_{L_z},L,L_z) = P_2\frac{L^2}{2} + P_1 U(\Theta_L,\Theta_{L_z},L_z/L,\phi_d), \tag{4}$$

where U is a periodic function of Θ_L,Θ_{L_z} of period π, and its exact form is presented in the Appendix.

The perturbing part in Eq. (4) contains several oscillating terms; however, the main resonance in our case is defined by requiring stationarity $\Phi \approx$ const of the phase mismatch $\Phi = 2(\Theta_L + \Theta_{L_z} - \phi_d)$. Assuming a weak drive, i.e., $P_1/P_2 \ll 1$ (this approximation is discussed in Sec. IV) in the vicinity of the resonance, we can use the single-resonance approximation [32], i.e., discard all the rapidly oscillating terms in the Hamiltonian. The resulting approximate, single-resonance Hamiltonian is (see Appendix)

$$H_r = P_2\frac{L^2}{2} + P_1 V\cos\Phi + P_1 F, \tag{5}$$

where

$$V = \frac{1}{8}\left(1 + \frac{L_z}{L}\right)^2, \tag{6}$$

$$F = \frac{1}{4}\left(1 - \frac{{L_z}^2}{L^2}\right). \tag{7}$$

The corresponding evolution equations are

$$\frac{d\Theta_L}{d\tau} = P_2 L - P_1\frac{L_z}{L^2}(V'\cos\Phi + F'), \tag{8}$$

$$\frac{d\Theta_{L_z}}{d\tau} = P_1\frac{1}{L}(V'\cos\Phi + F'), \tag{9}$$

$$\frac{dL}{d\tau} = 2P_1 V\sin\Phi, \tag{10}$$

$$\frac{dL_z}{d\tau} = 2P_1 V\sin\Phi. \tag{11}$$

Here, the prime denotes differentiation with respect to L_z/L. Equations (10) and (11) yield the integral of motion, $C = L - L_z$ $(0 \leqslant C \leqslant 2L)$, which allows reduction to a single

degree of freedom:

$$\frac{dL}{d\tau} = 2P_1 V \sin\Phi, \tag{12}$$

$$\frac{d\Phi}{d\tau} = 2P_2 L + 2P_1 \frac{C}{L^2}(V' \cos\Phi + F') - \tau. \tag{13}$$

Equation (9) still needs to be solved to obtain the precession of the angular momentum around the Z axis, but for calculating L, the one-degree-of-freedom set above is sufficient. This is our second (approximate) set used in the simulations below, which, due to the adiabaticity and reduced number of degrees of freedom, is considerably faster numerically than the full set of evolution equations in terms of the original spherical coordinates. We assume, and verify *a posteriori*, that if $\Delta L \ll 1$ is the range of L values in a persistent resonance with the drive in our problem, then $P_2 \Delta L \gg P_1$. Under this assumption, the second term in Eq. (13) can be neglected, and the phase-locking (resonance) condition $d\Phi/d\tau \approx 0$ yields $2P_2 L - \tau \approx 0$. Let $L_r(\tau) = \tau/2P_2 = \omega_d(\tau)/\omega_{\rm th}$ be the value of L satisfying the resonance condition exactly and define the deviation $\delta L = L - L_r$ from the exact resonance. The evolution equations then yield

$$\frac{d\delta L}{d\tau} = 2P_1 V \sin\Phi - \frac{1}{2P_2}, \tag{14}$$

$$\frac{d\Phi}{d\tau} = 2P_2 \delta L. \tag{15}$$

By taking the derivative of Eq. (15) with respect to time and inserting Eq. (14), we get

$$\frac{d^2\Phi}{d\tau^2} = -4P_1 P_2 V \sin\Phi - 1, \tag{16}$$

where we shifted Φ by π and, to lowest order in δL, $V \approx \frac{1}{8}(2 - \frac{C}{L_r})^2$ is evaluated at L_r. Equation (16) describes a pseudopendulum under the action of a constant torque. The Hamiltonian in this problem, with $d\Phi/d\tau$ acting as the momentum, is

$$H = \frac{1}{2}\left(\frac{d\Phi}{d\tau}\right)^2 + V_{\rm eff}(\Phi), \tag{17}$$

where

$$V_{\rm eff}(\Phi) = -4P_1 P_2 V \cos\Phi + \Phi. \tag{18}$$

This tilted cosine effective potential and the associated phase-space portrait of dynamics of the pseudopendulum are shown in Fig. 2 for $P_1 P_2 V = 0.75$. The phase space (bottom panel in the figure) is comprised of open and closed trajectories, provided $P_1 P_2 V > 1/4$. The open trajectories exhibit a continuous growth of the phase mismatch, i.e., they are not phase locked with the drive, while for the closed trajectories the phase mismatch is bounded. The closed trajectories are surrounded by the separatrix having area shown in red in the bottom panel of the figure. As $V(L_r)$ in our problem is slowly varying (increasing) in time, both the closed and open trajectories evolve adiabatically in time, unless near the separatrix. This means that deeply trapped trajectories remain trapped, i.e., the rotation frequency follows the drive, $L(\tau) \approx \omega_d(\tau)/\omega_{\rm th}$, constituting the AR in the system. The main problem remains the fate of the trajectories near the separatrix.

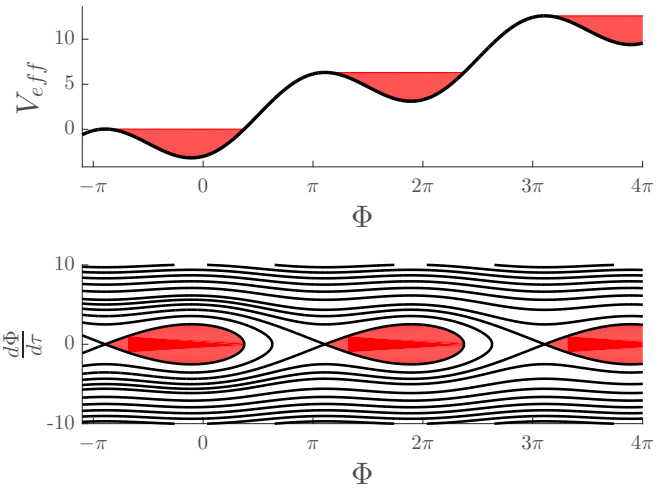

FIG. 2. The effective potential [Eq. (18)] (top) and the phase-space portrait of the associated dynamics (bottom). The boundary of the red filled area in the bottom panel is the separatrix. The value of $P_1 P_2 V$ was 0.75 and the equal energy lines in the bottom panel are separated by energy steps of π.

These trajectories, in principle, can change their trapping status as the result of nonadiabatic dynamics and, thus, affect the OC efficiency. It should be mentioned that many other AR systems [25–28] are described by the resonant Hamiltonian similar to Eq. (17). The process of capture into resonance in all these problems depends critically on the specific form of function V. In many such problems $V \sim \sqrt{I}$, where I is the relevant action variable in the problem. In all such cases, the capture into resonance from equilibrium and transition to AR is guaranteed provided the driving amplitude exceeds a sharp threshold [25]. Because of a different dependence of V on L no such threshold is characteristic of the driven molecule case. The study of this different capture mechanism comprises the main goal of the present investigation.

III. TRAPPING EFFICIENCY

A. The complexity of the resonant trapping problem

We have seen in simulations in Sec. II that for a range of parameters the OC yields controlled rotational excitation of molecular ensembles. Here we study the efficiency of such excitation process; i.e., we evaluate the fraction of molecules from some initial distribution, which are captured into and remain in resonance. Intuitively, one can assume that if the value of V changes adiabatically, molecules will be either trapped or not according to their initial location in phase space—inside or outside the separatrix. While the changes of V are generally adiabatic (as seen later), this intuition proves to be wrong. Indeed, the molecules which are inside the separatrix initially remain in resonance at later times, but additional molecules can cross the separatrix and enter the trapped region even if they were outside initially. An illustration of this process is presented in Fig. 3. Figure 3(a) shows the final phase-space distribution of a molecular ensemble having the same $L = 1$ and $C = 1$ initially and uniformly distributed values of Φ [see Fig. 3(b)]. The normalized driving frequency

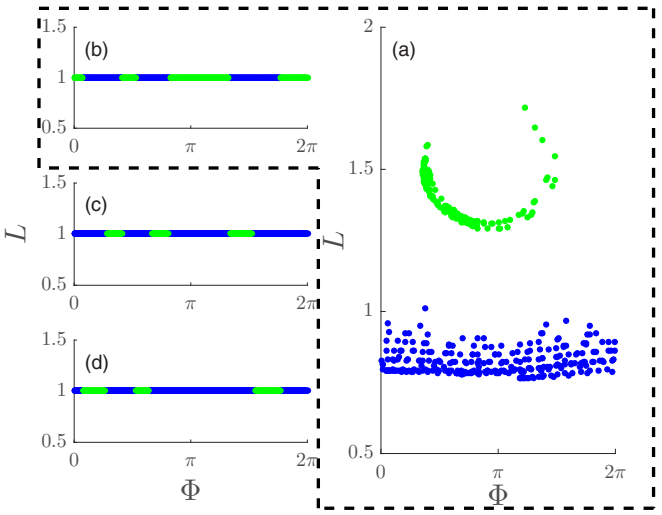

FIG. 3. Numerical simulations (single-resonance approximation) of passage through resonance with 500 molecules with initial $L_0 = 1$ and $C = 1$. All panels show the phase space (Φ, L), with green and blue circles representing resonantly trapped and untrapped molecules, respectively. The left panels show the initial distributions and differ by a small shift of the initial driving frequency: (b) $\omega_0 = 0.5$, (c) 0.49, and (d) 0.51. (a) Final distribution of the initial condition (b) at $\omega_f = 1.5$. The parameters are $P_1 = 1$, $P_2 = 10$, and Φ is shifted so that $\Phi = 0$ is at the saddle point (see Sec. III B).

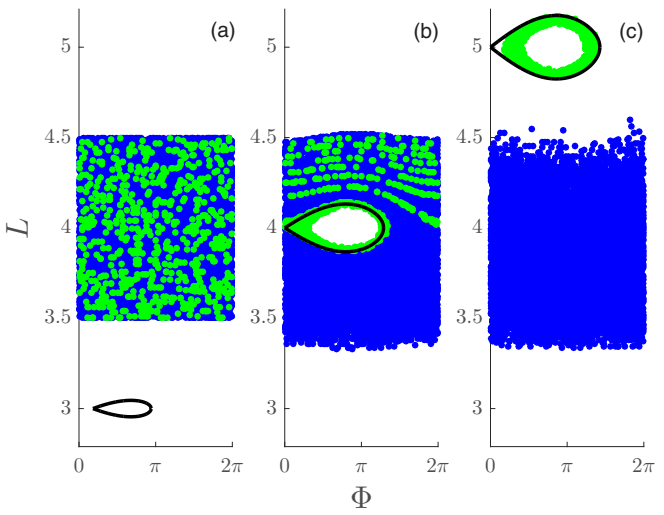

FIG. 4. Numerical simulations (single-resonance approximation) for 1×10^4 molecules distributed uniformly between $L = 3.5$ and 4.5 initially with $C = 4$. The panels show the distribution of the ensemble at three consecutive times (in terms of the normalized driving frequency): (a) $\omega_d = 3$, (b) 4, and (c) 5. Green and blue circles show resonantly trapped and untrapped molecules, respectively, and the black lines are the associated separatrices. The parameters are $P_1 = 0.63$ and $P_2 = 10$. Φ is shifted so that $\Phi = 0$ is at the saddle point of (c). A video of the simulation is provided in the Supplemental Material [35].

was varied from $\omega_0 = 0.5$ to $\omega_f = 1.5$, and one can see that, despite a much lower initial driving frequency compared to the rotation frequency of the molecules, a considerable number of molecules end up captured into resonance and rotationally accelerated (green). The location of the newly trapped molecules in the initial ensemble is shown in green in Fig. 3(b). We find that this location and the fraction of trapped molecules strongly depends on the initial value of the driving frequency. This complexity is illustrated in Figs. 3(c) and 3(d), showing in green the location of the molecules trapped in resonance with the drive for the same initial conditions, but with the initial driving frequency changed by ± 0.01. The fractions of the trapped molecules in Figs. 3(c) and 3(d) were 22% and 26%, respectively, compared to 46% in Figs. 3(a) and 3(b).

One approach to deal with the problem of nonadiabatic passage through the separatrix is to study an ensemble of initial conditions, checking whether the associated trajectories cross the separatrix. Previous works used such an approach with simpler systems, but the probabilistic nature of this nonadiabatic phenomenon led to rather complex results [33,34]. Here, we develop an alternative approach which examines the continuous phase-space dynamics of the initial ensemble instead of working with a collection of individual trajectories. This approach yields the resonant capture probability without ever specifying which initial conditions yield trajectories crossing the separatrix.

B. Phase-space dynamics

We base our analysis on Eq. (16), where $V = \frac{1}{8}(2 - \frac{C}{L})^2$ is evaluated at L_r and, therefore, both V and the associated separatrix area are monotonically increasing functions of time. For molecules close to the separatrix, trapped or untrapped, this approximation is satisfied because $\Delta L \ll 1$, where now we associate ΔL with the width of the separatrix in L. For untrapped molecules far from the separatrix we can still evaluate V at L_r, because the phase mismatch Φ for such molecules varies rapidly and the effect of the driving term in the quasipotential averages out. Next, instead of passage through resonance with an ensemble of molecules having the same value of L as illustrated in Fig. 3, we consider an ensemble of molecules with initially uniform density in phase space between $L_1 = 3.5$ and $L_2 = 4.5$ with all molecules having the same $C = 4$. We show a numerical simulation in such a system as the driving frequency (and therefore L_r) successively passes the resonance with all the molecules in the ensemble in Fig. 4 (a video of this simulation can be found in the Supplemental Material [35]). As the driving frequency sweeps through the ensemble [time progresses from Fig. 4(a) to Fig. 4(c)], the area of the associated separatrix (in black) increases and the added area is filled with the same density of molecules as in the original distribution. However, the area of the separatrix, which was empty when the separatrix first entered the distribution, remains empty, forming a phase-space hole passing through the distribution (similar phase-space holes were studied in plasma physics applications [36]). Note that the separatrix crossing occurs near the saddle point (where the adiabaticity condition is not met) and the molecules "line up" to enter the separatrix, as seen in Fig. 4(b). Following the crossing, the area filled by the newly trapped molecules is very regular, and the only irregular regions of phase space after passage through resonance are those near the boundaries $L_{1,2}$ of the

original distribution. Furthermore, one can observe that the whole distribution is shifted to lower values of L after the drive completed its passage through the ensemble.

The resonant phase-space dynamics shown in Fig. 4 can be explained on the bases of (a) the adiabaticity in the problem [37] and (b) the incompressibility of the phase space [38]. The adiabaticity guarantees the conservation of the area of the empty hole inside the growing separatrix, while the incompressibility of the phase space ensures that the distribution of the newly trapped molecules inside the separatrix would be the same uniform (original) distribution as long as L_r is well within the range L_1, L_2. Therefore, as time progresses and the resonant separatrix passes an infinitesimal distance δL_r inside the distribution, the density δN of newly trapped molecules is

$$\delta N = P\delta S = P\frac{\partial S}{\partial L_r}\delta L_r, \tag{19}$$

where P is the initial (uniform) density of the molecules in phase space and δS is the change of the area of the separatrix during the corresponding infinitesimal time interval. Thus, the number of newly trapped molecules after passage through the whole distribution is $\Delta N = P\Delta S$, ΔS being the full added area of the separatrix after the passage. These simple arguments also allow us to calculate the probability of capture into resonance for a general initial distribution of L and C (i.e., L_z), which is discussed next.

C. Capture probability

The generalization to the case of an arbitrary initial phase-space density distribution $P(L,C)$ independent of Φ can proceed by viewing this distribution as a collection of uniform infinitesimally thin layers, each having some value of C. As the most prevailing case, we focus on initially thermal distribution of molecules, where the distribution of L is

$$P_{\rm th}(L) = L\exp\left(-\frac{L^2}{2}\right), \tag{20}$$

and, therefore,

$$P(L,C) = \begin{cases} 0 & , \quad L < C/2 \\ \frac{NP_{\rm th}(L)}{4\pi L} & , \quad L > C/2, \end{cases} \tag{21}$$

where N is the density of the molecules. For a given C, we view this distribution as a collection of uniform layers of thickness δP as illustrated in Fig. 5. The resonant drive passes all these layers, so at any given time we have a collection of identical separatrices around the resonant L_r. Since the layers have a uniform density, and $\Delta L \ll 1$, the passage of the separatrix through the layers can be treated as discussed above. As the separatrix advances an infinitesimal distance δL_r, the total density (after summation over all the layers and integration over Φ) of newly trapped molecules for given C will be [see Eq. (19)]

$$\delta N(L_r,C) = P(L_r,C)\frac{\partial S}{\partial L_r}\delta L_r. \tag{22}$$

Next, we integrate Eq. (22) over C and change the integration from C to $R = L_z/L = 1 - C/L_r$, which is uniformly distributed between -1 and 1, to get

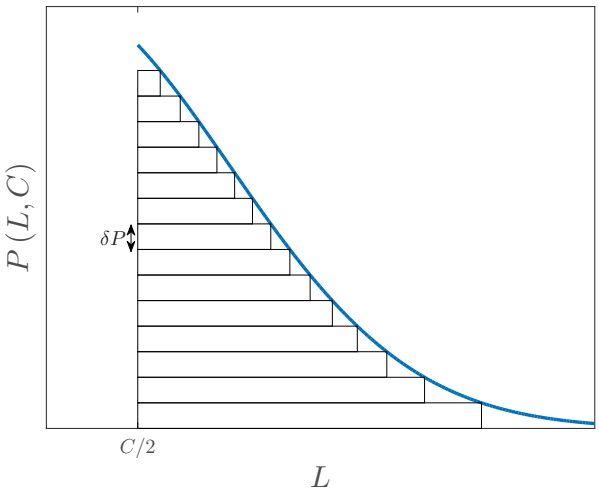

FIG. 5. Phase-space density distribution $P(L,C)$ viewed as a collection of uniform layers of height δP each.

$$\delta N(L_r) = \delta L_r\frac{NP_{\rm th}(L)}{4\pi L}\int_{-1}^{1}\frac{dS}{dR}(1-R)dR. \tag{23}$$

Finally, we collect the newly trapped molecules as the resonant L_r passes from some initial L_{r0} to a final value L_{rf} (the normalized driving frequency varies from ω_0 to ω_f) to get the density of all newly resonantly trapped molecules:

$$\Delta N = \int_{L_{r0}}^{L_{rf}}\frac{NP_{\rm th}(L)}{4\pi L}dL_r\int_{-1}^{1}\frac{dS}{dR}(1-R)dR. \tag{24}$$

After integrating in R (by parts) and in L_r, the last expression becomes

$$\Delta N = \sqrt{\frac{\pi}{2}}\frac{NQ}{4\pi}[\mathrm{erf}(\chi_f) - \mathrm{erf}(\chi_0)], \tag{25}$$

where $\chi = L_r/\sqrt{2} = \omega_d/(\sqrt{2}\omega_{\rm th})$ and $Q = \int_{-1}^{1} SdR$ is the total "volume" of the separatrix in the three-dimensional extended phase space which includes the R dimension. To get the total density of trapped molecules, we must add the density of the initially trapped molecules, which for $\Delta L \ll 1$ is

$$\Delta N_0 = \frac{QN}{4\pi}P_{\rm th}(\omega_0). \tag{26}$$

Then the total capture probability in the problem is

$$P_{\rm cap} = \frac{Q}{4\pi}\left\{\sqrt{\frac{\pi}{2}}[\mathrm{erf}(\chi_f) - \mathrm{erf}(\chi_0)] + P_{\rm th}(\omega_0)\right\}. \tag{27}$$

Finally, Q in the last equation can be found numerically via

$$Q = \frac{\sqrt{2}}{P_2}\int_{-1}^{1}dR\int_{\Delta\Phi}\sqrt{D(1-\cos\Phi) + \sin\Phi - \Phi}d\Phi, \tag{28}$$

where $D = \sqrt{[4P_1P_2V(R)]^2 - 1}$, $\Delta\Phi$ is the width of the separatrix in Φ, and we shifted Φ in Eq. (28) so that $\Phi = 0$ is at the saddle point. Note that Q depends on P_2 and the product P_1P_2 and, therefore, for a given ω_0, ω_f, the capture probability scales with temperature as $T^{-1/2}$ via P_2.

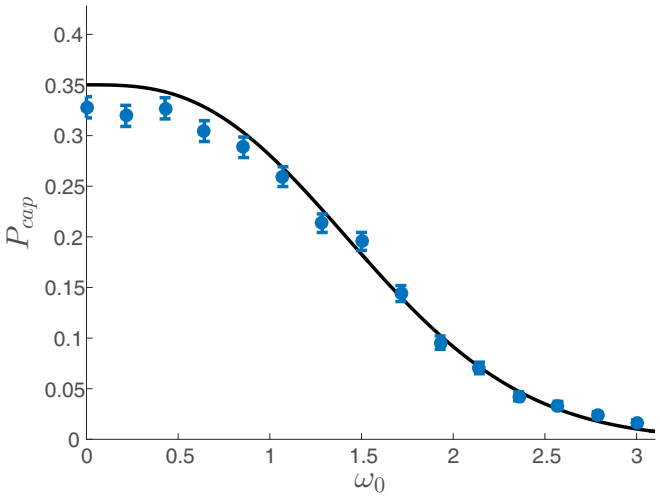

FIG. 6. Monte Carlo simulations (single-resonance approximation) of the resonant capture probability of an initially thermal ensemble (2000 molecules) versus the initial normalized driving frequency ω_0. The solid line is the analytic result [see Eq. (27)]. The parameters are $P_1 = 1.58$, $P_2 = 10$, and $\omega_f = 8$.

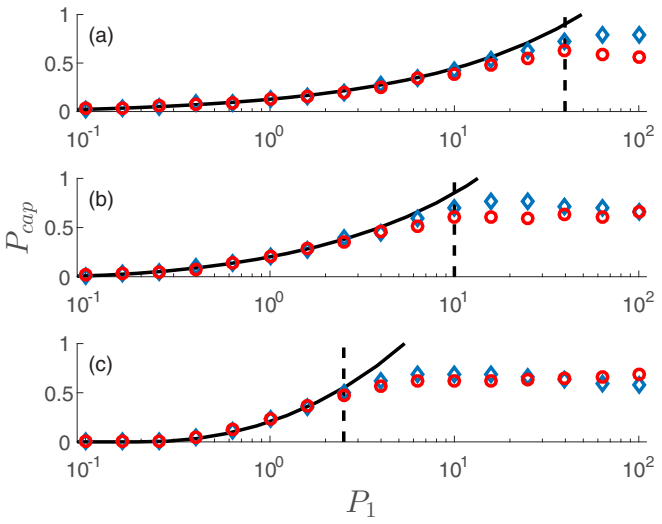

FIG. 7. The resonant capture probability for three equal P_2 lines in $P_{1,2}$ parameter space in Fig. 8. The red circles show full simulation in original spherical coordinates, blue diamonds are single-resonance simulations, and the analytic result is shown by the solid line. The parameters are (a) $P_2 = 39.8$, (b) 10, and (c) 2.51, with $\omega_0 = 1$ and $\omega_f = 5$. Dashed lines show the location of the weak drive limit. The number of molecules in simulations ranges from 500 to 5000, but the numerical uncertainty in all cases is smaller than the marker size.

Furthermore, asymptotically for large $P_1 P_2$, $Q \sim \sqrt{P_1/P_2}$, which is independent of the chirp rate β.

IV. RESULTS AND DISCUSSION

We illustrate our theory in Fig. 6, where the prediction of Eq. (27) is compared with numerical simulations (single-resonance approximation). We applied the OC drive to a thermal ensemble for parameters $P_1 = 1.58$, $P_2 = 10$. The final normalized driving frequency in this example was 8, while the initial normalized driving frequency was varied. One observes an excellent agreement of the theory (black line) with simulations. Note that counterintuitively, when ω_0 decreases and $P_{\rm th}(\omega_0)$ becomes small, the capture probability increases and reaches a maximum. In these cases, the vast majority of captured molecules cross the separatrix during the evolution and do not start in resonance initially.

Additional results are presented in Fig. 7, testing a broader range of parameters. In each panel in the figure, the OC drive with normalized frequency varying from $\omega_0 = 1$ to $\omega_f = 5$ is applied to a thermal ensemble and P_2 is kept constant at 39.8 [Fig. 7(a)], 10 [Fig. 7(b)], and 2.51 [Fig. 7(c)], while P_1 is varied. The numerical results include the simulations in spherical coordinates (blue diamonds), the single-resonance simulations (red circles), and both compared with the analytical result (solid line). One can see that the analytic prediction correctly describes the simulations only in a certain range of parameters. This is not surprising, as several approximations were made in the theory and need to be discussed next. One such approximation is the relative smallness $\Delta L \ll 1$ of the width of the separatrix in L. In terms of parameters $P_{1,2}$, this condition yields the inequality

$$\sqrt{P_1/P_2} \ll 1, \tag{29}$$

which justifies the approximation in Eq. (13). In addition, we used the single-resonance assumption, allowing us to discard higher nonresonant harmonic contributions in deriving Eq. (5), which requires $P_1/P_2 \ll 1$ and is guaranteed by Eq. (29). The location of $P_1 = P_2$ is shown in Fig. 7 by dashed lines and one can see that both types of simulations agree until one violates condition $P_1/P_2 \ll 1$, but the theoretical curves deviate earlier, because condition (29) is stricter. The ratio P_1/P_2 measures the relative strength of the drive, so Eq. (29) describes the weak drive limit.

Another assumption of the theory is the adiabaticity of autoresonant evolution, i.e., $\nu^{-2} d\nu/d\tau \ll 1$, where $\nu = \sqrt{4 P_1 P_2 V}$ is the characteristic frequency of autoresonant modulations (oscillations of trajectories trapped inside the separatrix). We estimate $d\nu/d\tau \sim O(\sqrt{P_1 P_2} dL_r/dt) \sim O(\sqrt{P_1/P_2})$ and, therefore the adiabaticity is guaranteed if

$$P_2 P_1^{1/3} \gg 1. \tag{30}$$

Note that the resonant capture is impossible when there is no separatrix (no trapped trajectories) for all C values, which leads to the condition

$$P_1 P_2 > 1/2 \tag{31}$$

for trapping. While this condition does not affect the validity of the results, it provides a useful border in $P_{1,2}$ parameter space. We summarize this analysis in Fig. 8 showing the $P_{1,2}$ parameter space with boundaries defined by the above conditions as black solid lines and the region of validity of the analytic results in color with the color map corresponding to the theoretical capture probability for $\omega_0 = 1$ and $\omega_f = 5$. The black diamond in the figure shows the conditions of experiments [16,17,39] ($E_0 \approx 4.3 \times 10^9$ V/m, $\beta \approx 1.7 \times 10^{24}$ s^{-2} for O_2 molecules at room temperature), which are in the region of validity of the theory. The red dashed lines mark the parameter range

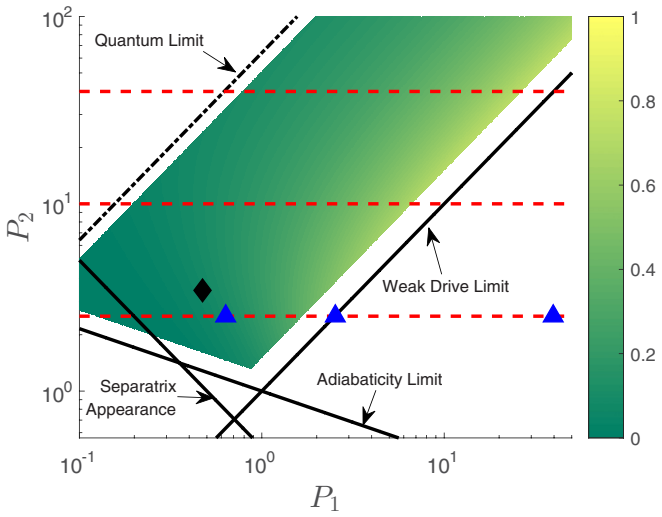

FIG. 8. Validity conditions in $P_{1,2}$ parameter space. The color coding represents the capture probability for a drive with $\omega_0 = 1$, $\omega_f = 5$. The black lines are the weak drive limit [Eq. (29)], location of formation of the separatrix [Eq. (31)], and the adiabaticity condition [Eq. (30)]. The dash-dotted black line is an example of the quantum limit for O_2 at room temperature. The horizontal red dashed lines represent the values of $P_{1,2}$ simulated in Fig 7. The blue triangles are the parameters used in Fig. 1, while the black diamond shows parameters used in experiments [16,17,39].

in simulations in Fig. 7, while the blue triangles show the conditions of simulations in Fig. 1, where panel (c) is way outside the weak drive limit.

At this stage, we discuss the assumed classicality of our system. The classical thermal distribution (20) is valid only when the most probable j, the quantum number associated with the total angular momentum, in the thermal equilibrium is large, say $j_{\rm th} > 5$. In addition, the dynamics of trapped molecules must be classical. For this to be true, the characteristic area S (dimensional) of the separatrix in phase space must exceed Planck's constant h, so mixing of a few angular momentum states would be possible. Then, the inequality $\sqrt{P_2/P_1} < j_{\rm th}$ can serve as a condition for classicality of trapped trajectories. An example of this condition is presented in Fig. 8 by the dot-dashed line for O_2 at room temperature. Unlike the rest of the above conditions, this line is not fixed in the $P_{1,2}$ space and is both temperature and molecule dependent via $j_{\rm th}$ ($j_{\rm th} = 9$ in the figure). Note that the classical results presented in this work are in the range of typical OC experiments. Note also that the conservation law $L - L_z = \text{const}$ in our theory is the classical counterpart of the OC quantum selection rule $|j,m\rangle \to |j+2,m+2\rangle$, where m is the magnetic quantum number [22].

Finally, in developing the theory, we have assumed that the characteristic parameters $P_{1,2}$ are constant. In typical experiments these parameters may vary in time. For example, the laser-pulse amplitude may have slow temporal dependence, the chirp rate β may vary in time, and the trapped molecules may experience slow centrifugal expansion at high rotation speeds. Because of the adiabaticity, these effects can be taken into account within our theory by using instantaneous values of $P_{1,2}$. For example, the adiabaticity guarantees continued trapping in the system as long as $P_1 P_2 V$ [see Eq. (16)] is an increasing function of time. If this function starts to decrease because of the aforementioned variation of parameters, some molecules can escape the trapping. This effect of "leaked molecules" was recently observed experimentally [16,17]. Note that this leakage can be stopped by slowly increasing the driving amplitude, i.e., P_1, in time.

V. SUMMARY

In conclusion, we have studied the process of capture of an ensemble of molecules into resonance in the optical centrifuge and calculated the associated capture probability. Based on three characteristic time scales in the problem, we have introduced two dimensionless parameters $P_{1,2}$ [see Eqs. (1) and (2)], transformed the problem to action-angle representation, and applied the single-resonance approximation in our analysis, allowing a significant acceleration of numerical simulations. We have then studied the continuous phase-space dynamics of the reduced one-degree-of-freedom system and found the probability of filling of separatrix by newly trapped molecules. This calculation was based on the adiabaticity in the problem and the incompressibility of the phase space, avoiding the complex issue of deciding the fate of individual trajectories. For a thermal ensemble, we have compared the analytic results with numerical simulations, showing excellent agreement, provided one satisfies the weak drive limit, the adiabaticity, and the classicality conditions, which were mapped in $P_{1,2}$ parameter space. It is shown that these conditions hold in current experimental setups. The results of this work can be used in analyzing existing and planning future experiments. It also seems important to generalize the theory into the quantum regime and study the transition from the quantum ladder climbing to the classical autoresonance [29,40] in the problem of molecular rotations. Finally, a similar phase-space analysis can be applied in studying the problem of capture into autoresonance in other dynamical systems.

ACKNOWLEDGMENT

This work was supported by the Israel Science Foundation Grant No. 30/14.

APPENDIX

The transformation to action-angle variables discussed in Sec. II is carried out similarly to [41,42]. We proceed by solving the Hamilton-Jacobi equation in the problem to obtain the generating function [41]

$$W(L,L_z,\varphi,\theta) = \pm \int \sqrt{L^2 - \frac{L_z^2}{\sin^2\theta}}\, d\theta + \varphi L_z, \qquad \text{(A1)}$$

where the actions are the angular momentum L and its projection L_z on the Z axis, the integration is along the trajectory, and the choice of the sign accounts for the difference between the ascending and descending nodes. The canonical transformation equations in this case are

$$p_\varphi = \frac{\partial W}{\partial \varphi} = L_z, \qquad \text{(A2)}$$

$$p_\theta = \frac{\partial W}{\partial \theta} = \pm\sqrt{L^2 - \frac{L_z^2}{\sin^2\theta}}, \tag{A3}$$

$$\Theta_L = \frac{\partial W}{\partial L} = \pm\int \frac{L\sin\theta}{\sqrt{L^2\sin^2\theta - L_z^2}}d\theta, \tag{A4}$$

$$\Theta_{L_z} = \frac{\partial W}{\partial L_z} = \mp\int \frac{L_z}{\sin^2\theta}\frac{1}{\sqrt{L^2 - \frac{L_z^2}{\sin^2\theta}}}d\theta + \varphi. \tag{A5}$$

It was shown in [41] that the angles Θ_L, Θ_{L_z} are two of the Euler angles, and Θ_L measures the rotation of the molecule in its plane of rotation while Θ_{L_z} measures the precession of the rotation plane itself. Substitution of the first two transformation equations into the unperturbed Hamiltonian yields

$$H_0 = P_2 L^2/2. \tag{A6}$$

For calculating the perturbed part of the Hamiltonian we set $\Theta_L = 0$ when θ is at its minimal value, and $\Theta_{L_z} = 0$ when the line of nodes is along the X axis, and solve the integrals in Eqs. (A4) and (A5) to find

$$\cos\theta = \sqrt{1 - L_z^2/L^2}\cos\Theta_L, \tag{A7}$$

$$\varphi = \Theta_{L_z} + \arctan[(L/L_z)\tan\Theta_L] + \frac{\pi}{2}. \tag{A8}$$

Next, we define $s = \mathrm{sign}L_z$ and notice that $\arctan(L/L_z\tan\Theta_L)$ can be written as the sum $s\Theta_L + sf(|L/L_z|,\Theta_L)$, where f is a periodic function of Θ_L of period π. We expand this function in Fourier series to get

$$f(|L/L_z|,\Theta_L) = \sum_{n=1}^{\infty}\frac{(|L/L_z|-1)^n}{n(|L/L_z|+1)^n}\sin(2n\Theta_L), \tag{A9}$$

which, in terms of $A = (|L/L_z|-1)/(|L/L_z|+1)$, becomes

$$f(|L/L_z|,\Theta_L) = -\frac{i}{2}\ln\left(\frac{1 - Ae^{-2i\Theta_L}}{1 - Ae^{2i\Theta_L}}\right). \tag{A10}$$

At this point, we write the action-angle representation of the perturbed part of the Hamiltonian using Eqs. (A7) and (A8):

$$U = \left[\left(1 - L_z^2/L^2\right)\cos^2\Theta_L - 1\right]\sin^2\Psi, \tag{A11}$$

where $\Psi = \Theta_{L_z} + s\Theta_L + sf - \phi_d$, and then we use Eq. (A10) to find the closed-form expressions for $\cos(2f)$, $\sin(2f)$. We define the phase mismatch $\Phi = 2(\Theta_L + \Theta_{L_z} - \phi_d)$ in the problem, use this definition to replace $2(\Theta_{L_z} - \phi_d)$ in Eq. (A11), and average the resulting $U(L_z/L,\Theta_L,\Phi)$ with respect to the fast phase Θ_L. This yields the full Hamiltonian in the single-resonance approximation:

$$H(\Theta_L,\Theta_{L_z},L,L_z) \approx P_2\frac{L^2}{2} + P_1 V\cos\Phi + P_1 F, \tag{A12}$$

where

$$V = \frac{1}{8}\left(1 + \frac{L_z}{L}\right)^2, \tag{A13}$$

$$F = \frac{1}{4}\left(1 - \frac{{L_z}^2}{L^2}\right). \tag{A14}$$

Note that this result is independent of s and that angle Θ_L exhibits nontrivial behavior, as it always increases, regardless the direction of rotation (given by s).

[1] I. S. Averbukh and R. Arvieu, Phys. Rev. Lett. **87**, 163601 (2001).
[2] F. Rosca-Pruna and M. J. J. Vrakking, Phys. Rev. Lett. **87**, 153902 (2001).
[3] J. M. Rost, J. C. Griffin, B. Friedrich, and D. R. Herschbach, Phys. Rev. Lett. **68**, 1299 (1992).
[4] M. J. J. Vrakking and S. Stolte, Chem. Phys. Lett. **271**, 209 (1997).
[5] K. Kitano, H. Hasegawa, and Y. Ohshima, Phys. Rev. Lett. **103**, 223002 (2009).
[6] S. Fleischer, Y. Khodorkovsky, Y. Prior, and I. S Averbukh, New J. Phys. **11**, 105039 (2009).
[7] S. Zhdanovich, A. A. Milner, C. Bloomquist, J. Floss, I. Sh. Averbukh, J. W. Hepburn, and V. Milner, Phys. Rev. Lett. **107**, 243004 (2011).
[8] J. Karczmarek, J. Wright, P. Corkum, and M. Ivanov, Phys. Rev. Lett. **82**, 3420 (1999).
[9] D. M. Villeneuve, S. A. Aseyev, P. Dietrich, M. Spanner, M. Yu. Ivanov, and P. B. Corkum, Phys. Rev. Lett. **85**, 542 (2000).
[10] R. Hasbani, B. Ostojic, P. R. Bunker, and M. Y. Ivanov, J. Chem. Phys. **116**, 10636 (2002).
[11] K. Tilford, M. Hoster, P. M. Florian, and R. C. Forrey, Phys. Rev. A **69**, 052705 (2004).
[12] Y. Khodorkovsky, J. R. Manson, and I. Sh. Averbukh, Phys. Rev. A **84**, 053420 (2011).
[13] U. Steinitz, Y. Prior, and I. S. Averbukh, Phys. Rev. Lett. **112**, 013004 (2014).
[14] U. Steinitz, Y. Prior, and I. S. Averbukh, Phys. Rev. Lett. **109**, 033001 (2012).
[15] L. Yuan, S. W. Teitelbaum, A. Robinson, and A. S. Mullin, Proc. Natl. Acad. Sci. USA **108**, E17 (2011).
[16] A. Korobenko, A. A. Milner, and V. Milner, Phys. Rev. Lett. **112**, 113004 (2014).
[17] A. A. Milner, A. Korobenko, J. W. Hepburn, and V. Milner, Phys. Rev. Lett. **113**, 043005 (2014).
[18] A. A. Milner, A. Korobenko, K. Rezaiezadeh, and V. Milner, Phys. Rev. X **5**, 031041 (2015).
[19] A. A. Milner, A. Korobenko, and V. Milner, Opt. Express **23**, 8603 (2015).
[20] M. Spanner and M. Y. Ivanov, J. Chem. Phys. **114**, 3456 (2001).
[21] M. Spanner, K. M. Davitt, and M. Y. Ivanov, J. Chem. Phys. **115**, 8403 (2001).
[22] N. V. Vitanov and B. Girard, Phys. Rev. A **69**, 033409 (2004).
[23] B. Meerson and L. Friedland, Phys. Rev. A **41**, 5233 (1990).

[24] W. K. Liu, B. Wu, and J. M. Yuan, Phys. Rev. Lett. **75**, 1292 (1995).
[25] J. Fajans, E. Gilson, and L. Friedland, Phys. Rev. Lett. **82**, 4444 (1999).
[26] J. Fajans, E. Gilson, and L. Friedland, Phys. Plasmas **6**, 4497 (1999).
[27] L. Friedland, Phys. Rev. E **59**, 4106 (1999).
[28] G. Manfredi and P. A. Hervieux, Appl. Phys. Lett. **91**, 061108 (2007).
[29] G. Marcus, L. Friedland, and A. Zigler, Phys. Rev. A **69**, 013407 (2004).
[30] Y. Shalibo, Y. Rofe, I. Barth, L. Friedland, R. Bialczack, J. M. Martinis, and N. Katz, Phys. Rev. Lett. **108**, 037701 (2012).
[31] I. Barth and L. Friedland, Phys. Rev. Lett. **113**, 040403 (2014).
[32] B. V. Chirikov, Phys. Rep. **52**, 263 (1979).
[33] J. Fajans, E. Gilson, and L. Friedland, Phys. Rev. E **62**, 4131 (2000).
[34] A. I. Neishtadt, in *Mathematics and modelling*, edited by A. Bazykin and Yu. Zarkhin (Nova Science, Commack, NY, 1993), pp. 199-226.
[35] See Supplemental Material at http://link.aps.org/supplemental/10.1103/PhysRevA.93.043406 for a video of the simulation in Fig. 4.
[36] L. Friedland, P. Khain, and A. G. Shagalov, Phys. Rev. Lett. **96**, 225001 (2006).
[37] L. D. Landau and E. M. Lifshits, *Mechanics* (Pergamon, Oxford, U.K., 1976), pp. 154–157.
[38] H. Goldstein, *Classical Mechanics* (Addison-Wesley, Reading, MA, 1980), pp. 426–428.
[39] A. A. Milner, A. Korobenko, and V. Milner, New J. Phys. **16**, 093038 (2014).
[40] I. Barth and L. Friedland, Phys. Rev. A **87**, 053420 (2013).
[41] H. Goldstein, *Classical Mechanics* (Addison-Wesley, Reading, MA, 1980), pp. 472–483.
[42] E. Grosfeld and L. Friedland, Phys. Rev. E **65**, 046230 (2002).